ARTICLES
https://doi.org/10.1038/s41567-020-01112-z

nature physics

Measurement-induced topological entanglement transitions in symmetric random quantum circuits

Ali Lavasani[1,2] ✉, Yahya Alavirad[1,2] and Maissam Barkeshli[1,2]

Random quantum circuits, in which an array of qubits is subjected to a series of randomly chosen unitary operations, have provided key insights into the dynamics of many-body quantum entanglement. Recent work has shown that interleaving the unitary operations with single-qubit measurements can drive a transition between high- and low-entanglement phases. Here we study a class of symmetric random quantum circuits with two competing types of measurement in addition to unitary dynamics. We find a rich phase diagram involving robust symmetry-protected topological, trivial and volume law entangled phases, where the transitions are hidden to expectation values of any operator and are only apparent by averaging the entanglement entropy over quantum trajectories. In the absence of unitary dynamics, we find a purely measurement-induced critical point, which maps exactly to two copies of a classical two-dimensional percolation problem. Numerical simulations indicate that this transition is a tricritical point that splits into two critical lines in the presence of arbitrarily sparse unitary dynamics with an intervening volume law entangled phase. Our results show that measurements alone are sufficient to induce criticality and logarithmic entanglement scaling, and arbitrarily sparse unitary dynamics can be sufficient to stabilize volume law entangled phases in the presence of rapid, yet competing, measurements.

Generic unitary dynamics drive quantum many-body systems into highly entangled states characterized by volume law scaling of subsystem entanglement entropies. When this dynamics is intercepted by rapid local measurements, individual quantum trajectories are expected to collapse into low-entanglement states characterized by area law scaling of subsystem entanglement entropies. Recently, it was discovered that, at least in a class of models, these two phases are separated by a scale-invariant 'critical point' at a finite measurement rate[1–3]. Several aspects of this transition and its generalizations have been studied recently[4–19].

In the limit of infinitely rapid local measurements, the state of the system crucially depends on the choice of measurement basis. Assuming one measures only commuting single-qubit operators, the wavefunction collapses into an unentangled trivial product state. However, if one chooses to measure a set of stabilizer operators that stabilize a topological or a symmetry-protected topological (SPT) wavefunction, the resulting state—despite also having area law scaling of entanglement—would be topologically distinct from the product state[20,21].

In this Article, we consider the competition between these two types of measurement with each other, as well as with the unitary dynamics. This raises the question of whether the notion of a topological phase is well defined in random quantum circuits that include both unitary dynamics and local measurements. To make progress in answering this question, we consider a $(1+1)$D quantum circuit model comprising three elements: (1) measurement of stabilizer operators that stabilize a $\mathbb{Z}_2\times\mathbb{Z}_2$ SPT realized by the 'cluster model'[22,23]; (2) single-qubit measurements in the computational basis; (3) random, symmetry-allowed Clifford unitary gates. At each step of the circuit, one element is selected at random with probabilities p_t, p_s and p_u respectively ($p_t+p_s+p_u=1$) and applied at a random position in space. A typical snapshot of the circuit is shown in Fig. 1a.

Using suitably defined order parameters, we discover a rich phase diagram, shown in Fig. 1b. We find not only a stable SPT phase in an extended region of the phase diagram, but our results indicate a tricritical point, with logarithmic scaling of entanglement entropy separating the volume law, trivial and SPT phases in the absence of unitary dynamics $p_u=0$; that is, when only measurements are present. The existence of this tricritical point implies that a volume law phase can be stabilized by an infinitesimally small rate of unitary dynamics.

Moreover, we find an exact analytical mapping that maps the case without unitary dynamics $p_u=0$ to two copies of a (non-standard) classical 2D percolation problem. Away from the $p_u=0$ line, we extensively study the phase transitions numerically. The numerical results are consistent with the correlation length critical exponent ν remaining the same on the phase boundaries all the way down to the tricritical point, which has $\nu=4/3$ based on the analytical mapping to percolation. On the other hand, we find that the coefficient of the logarithmic scaling of the entanglement entropy changes considerably, suggesting that the conformal field theory (CFT) description changes along the phase boundaries.

Model

We study a family of $(1+1)$D random quantum circuits that realize quantum trajectories extrapolating between wavefunctions in an SPT phase, a trivial product state and a volume law entangled phase.

We choose our SPT to be the $\mathbb{Z}_2\times\mathbb{Z}_2$ symmetry-protected phase realized by the cluster model defined on an open chain of N qubits (where N is even throughout) in $(1+1)$D (refs. [22,23]):

$$H_0 = -\sum_{i=2}^{N-1} X_{i-1}Z_iX_{i+1} \tag{1}$$

where X_i and Z_i denote Pauli matrices. Note that all terms commute with each other and this model is therefore exactly solvable. This model realizes a SPT phase[24–26] protected by the $\mathbb{Z}_2\times\mathbb{Z}_2$ symmetry generated by

[1]Department of Physics, Condensed Matter Theory Center, University of Maryland, College Park, MD, USA. [2]Joint Quantum Institute, University of Maryland, College Park, MD, USA. ✉e-mail: seyedali@umd.edu

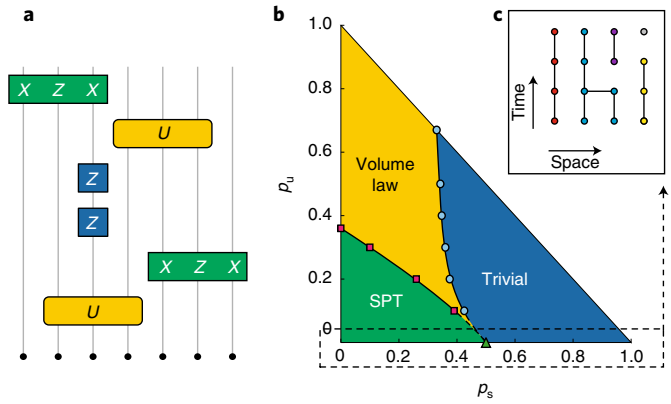

Fig. 1 | Schematic of the circuit and its corresponding phase diagram. **a**, Schematic of a typical quantum circuit. Yellow boxes correspond to a three-qubit random Clifford unitary, blue and green boxes represent projective measurements. **b**, Phase diagram describing the entanglement structure of the steady state. Red squares and blue circles are obtained from numerical simulations, whereas the rest of the phase boundaries are extrapolated. **c**, Mapping the dynamics of the random circuit on the $p_u = 0$ axis to the 2D percolation on a square lattice. Each cluster is assigned a unique colour and qubits of the same colour make up their own SPT state (see Proposition 1 for details).

$$G_1 = \prod_{i \text{ is even}} Z_i \,;\; G_2 = \prod_{i \text{ is odd}} Z_i. \tag{2}$$

We say that an eigenstate of H_0 is a symmetry-invariant eigenstate if it is an eigenstate of all terms in H_0 as well as G_1 and G_2. All symmetry-invariant eigenstates within the same symmetry sector can be related to each other by a symmetry-preserving constant-depth local unitary circuit.

On an open chain, a particular generalization of entanglement entropy[23,27–29] can be used as an order parameter for this SPT phase. Consider dividing the system as shown in Fig. 2. The generalized topological entanglement entropy S_{topo} is defined as

$$S_{\text{topo}} \equiv S_{\text{AB}} + S_{\text{BC}} - S_{\text{B}} - S_{\text{ABC}}. \tag{3}$$

S_{AB} is the von Neumann entanglement entropy of the region A ∪ B in the chain. Other terms are defined similarly. One can show that for all symmetry-invariant eigenstates of H_0, $S_{\text{topo}} = 2$.

To realize a wavefunction in this SPT phase (that is, a symmetry-invariant eigenstate of H_0), we can, for example, use a quantum circuit that starts with an arbitrary eigenstate of G_1 and G_2 and then proceed to measure all stabilizer operators $g_i \equiv X_{i-1}Z_iX_{i+1}$.

To realize wavefunctions in the trivial phase, we use a quantum circuit that measures all single-qubit operators in the Z_i basis. The choice of the single-qubit measurement basis Z_i is fixed by requiring that all measurement operators commute with the symmetry generators G_1 and G_2 (see Supplementary Section 1 for the case with symmetry-violating measurements). All wavefunctions in the trivial phase have $S_{\text{topo}} = 0$.

To realize wavefunctions in the volume law phase, we use random Clifford unitary gates that are allowed by the symmetry. The simplest class of gate to consider would be two-qubit nearest-neighbour random unitaries. However, due to the symmetry restrictions, this set is not effective in entangling the qubits. Ergo, we work with three-qubit random unitary gates.

We are now in a position to construct our full quantum circuit model: we start with the $|0\rangle^{\otimes N}$ state. In each updating step, we either: (1) apply a random three-qubit Clifford unitary between qubits $i-1$, i and $i+1$ with probability p_u, for a random i drawn from 2, ⋯ , $N-1$; (2) measure the single-qubit operator Z_i with probability p_s for a random i drawn from 1, ⋯ , N; or (3) measure the stabilizer $g_i \equiv X_{i-1}Z_iX_{i+1}$ with probability $p_t = 1 - p_s - p_u$ for a random i drawn from 2, ⋯ , $N-1$. A time step is defined as N consecutive updating steps.

In the limiting case $p_u = 1$ and $p_s = 0$, the random unitary circuit drives the system into a volume law phase, whereas for the other two limiting cases—that is, $p_u = 0$, $p_s = 0$ and $p_u = 0$, $p_s = 1$—the system is in an area law phase, one with SPT order and the other without.

We detect the presence of the different phases in several distinct ways. First, at each time step we calculate S_{topo}, averaged over quantum trajectories, and run the circuit until a steady-state value is obtained. To detect the phase transition from the area law phase to the volume law phase, we also extensively use the order parameter originally introduced in ref. [6]; to do so, we first run the circuit for time $2N$ to reach the steady state. Then we entangle an ancilla qubit with the two qubits in the middle of the chain by measuring the following stabilizers:

$$Z_{N/2-1}Z_{\text{a}}, \quad Z_{N/2+1}Z_{\text{a}}, \quad X_{N/2-1}X_{\text{a}}X_{N/2+1}, \tag{4}$$

where X_a and Z_a act on the ancilla qubit. Note that all three stabilizers commute with the symmetry generators G_1 and G_2. Next, we let the circuit run for an extra $O(N)$ time steps, and then measure the entanglement entropy of the ancilla qubit, denoted by S_a. Here, $O(N)$ stands for linear time in N. As shown in ref. [6], if the system is in the area law phase, the ancillla's entanglement entropy S_a should be zero by the time we measure it, whereas in a volume law phase, the ancilla should be still entangled with the system.

We also use a slightly modified version of the ancilla order parameter[6], which we call the scrambled ancilla order parameter denoted by $\tilde{S}_a$, such that instead of one ancilla we use ten, and instead of measuring the stabilizers listed in equation (4), the ancillas are entangled with the system via ten time steps of a scrambling circuit, where at each updating step a random (non-symmetric) three-qubit Clifford gate is applied to three randomly drawn qubits. As was the case for S_a, we measure the entropy of the ancilla subsystem after the qubit chain evolves $O(N)$ time steps under the symmetric random circuit. While in the trivial phase, the ancilla subsystem would have been entirely disentangled from the qubit chain, giving $\tilde{S}_a = 0$, whereas in the SPT phase, the ancilla subsystem should have remained entangled with the two edge degrees of freedom that are protected by the symmetry, resulting in $\tilde{S}_a = 2$. In the volume law phase, the ancilla subsytem should remain entangled with the bulk as well and hence $\tilde{S}_a > 2$.

Compared with $\tilde{S}_a$ and S_{topo}, S_a shows a sharper SPT phase to volume law phase transition when $p_u > 0$ (Supplementary Section 11)—and hence it is used to extract the corresponding critical exponents—but is unable to detect the topological phase transition at $p_u = 0$. On the other hand, $\tilde{S}_a$ can be used as an experimentally accessible probe to detect the phase transition at $p_u = 0$.

We note that a type of Edwards–Anderson glass order parameter can also be used to detect the topological phase (Supplementary Section 4), although it cannot distinguish the trivial and volume law phases.

Finally, we note that the random quantum circuits studied here, viewed as a quantum channel, eventually transform the initial state of the system into the maximally mixed state allowed by the symmetry (see Supplementary Section 3 for a proof and a bound on how fast this happens). The steady-state expectation value of any operator therefore stays the same throughout the phase diagram and thus cannot serve as an order parameter.

Mapping the case without unitary dynamics $p_u = 0$ to classical percolation

Here we show how to map the entire $p_u = 0$ line in the random circuit presented above to two copies of a classical 2D percolation problem

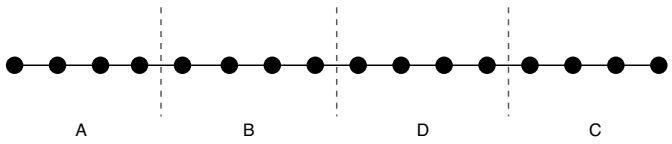

Fig. 2 | Chain cuts used to define the generalized topological entanglement entropy. The A, B and C regions that are used to define S_{topo} (equation (3)) are marked; S_{topo} basically measures the quantum conditional mutual information I(A: C|B) (note that the labels are not in alphabetical order).

on a square lattice. This percolation model is non-standard, although our numerical results indicate that it has the same critical properties as the standard classical percolation model on the square lattice. There is a distinct, but closely related, random quantum circuit that we define in Supplementary Section 9 that does map directly to (two copies of) standard classical percolation.

We divide the operators measured by the random circuit into two sets. One set, which we call the odd site operators, is comprised of single-qubit operators Z_i for odd i alongside the stabilizers g_j, which end on the odd sites; that is, for even j. The even site operators are defined analogously. Note that each member of one set commutes with all elements of the other set.

Let us focus on the measurements of odd site operators. Consider the $N/2\times M$ square lattice shown in Fig. 1c, where M is the total number of updating steps in the circuit. We call this lattice the odd sites' percolation lattice. The $N/2$ vertices on each row correspond to the odd sites of the system and we label them accordingly. The vertical (horizontal) links ending (residing) on the mth row are related to the Z_i (g_j) measurements in the mth step of the circuit in the following way: if Z_i is not measured at updating step m, we draw a vertical link between the $(i, m-1)$ and (i, m) vertices. If the stabilizer g_j is measured at step m, we also draw a horizontal link between the $(j-1, m)$ and $(j+1, m)$ vertices. At the end, we assign a unique colour to each connected cluster of vertices. We construct the even sites' percolation lattice analogously. The randomness of the quantum circuit translates into random connections in the percolation lattices; the probability distributions for the links in the percolation lattice are detailed in Supplementary Section 5.

The entanglement structure of the system at step M can be extracted from the colours of the vertices on the last row of the two aforementioned percolation lattices. As the following proposition specifies, qubits of the same colour make up their own SPT state.

Proposition 1. Group the qubits on the basis of their colour on the last row of the percolation lattice. Let $A^j = \{q_i\}_{i=1}^n$ denote the ordered set of qubit indices corresponding to jth colour; that is, q_i label a set of qubits that are all the same colour at step M. Then, up to a minus sign, the operators that stabilize the state of the system at step M are of the following form

$$\prod_{i=1}^{n} Z_{q_i} \quad \text{and} \quad g_{q_i,q_{i+1}} \quad \text{for } i = 1, 2, \cdots n-1, \tag{5}$$

where $g_{q_i,q_{i+1}}$ is defined as

$$g_{i,j} = X_i \left[\prod_{k=0}^{\frac{j-i}{2}-1} Z_{i+2k+1}\right] X_j. \tag{6}$$

By considering similarly defined stabilizer operators for all of the different colours (A^j with different j), we get a complete set of stabilizers that specify the state of the system. The proof of Proposition 1 is presented in Supplementary Section 8.

As shown in Lemma 1 in Supplementary Section 2, the minus sign ambiguity in Proposition 1 has no bearing on the entanglement spectrum of the system's state. Thus the percolation lattices exactly determine the (von Neumann or Rènyi) entanglement entropy for any subset of qubits.

Numerical results

We start by briefly reviewing the quantities we numerically calculate to obtain the phase diagram and to characterize the critical phase boundaries.

A signature of criticality in (1+1)D systems is the logarithmic scaling of the entanglement entropy. Thus, we calculate the entanglement entropy at the tth time step (which corresponds to tN updating steps) $S(x, L; t)$ of a subsystem of length x for a system of total length $L=N$, averaged over all of the quantum trajectories of the circuit.

In the large time limit, this averaged entanglement entropy saturates to a logarithmic form at the phase transitions as in (1+1)D CFTs[30]:

$$S(x, L) = a_x \log\left(\frac{L}{\pi}\sin\frac{\pi x}{L}\right) + b. \tag{7}$$

We can also characterize the entanglement growth with time. At criticality, for timescales much smaller than the saturation time, we have

$$S(x, L; t) = a_t \log(t) + b'. \tag{8}$$

Note that contrary to unitary CFTs, the coefficient of the logarithmic scaling a_x is not given by the central charge of any underlying CFT. In the context of the area law to volume law transition, ref. [31] provides an appealing interpretation of a_x and a_t as universal quantities given by the scaling dimension of certain 'boundary condition changing' operators; b and b' are non-universal constants.

Throughout the phase boundaries, we find $a_x = a_t$ within the margin of error, which is consistent with a dynamical exponent $z=1$, as the entanglement growth rate is similar along the time and space directions.

We can use S_{topo} as the order parameter to distinguish the three different phases: S_{topo} would be extensive in the volume law phase, whereas in the thermodynamic limit it should converge to values 2 and 0 in the topological and trivial phases, respectively. Let $S_{topo}(p, L)$ denote the steady-state value of S_{topo} when some tuning parameter (for example, the single-qubit measurement probability) is p and system size is L. On general grounds, we expect the following scaling form in the vicinity of the critical point:

$$S_{topo}(p, L) = F\Big((p - p_c)L^{1/\nu}\Big), \tag{9}$$

where $F(x)$ is some unknown function, p_c is the critical value of tuning parameter p and ν is the correlation length critical exponent, $\xi \propto |p - p_c|^{-\nu}$.

As explained in the 'Model' section, the entanglement entropy of a suitably entangled ancilla system, S_a or $\tilde{S}_a$, can also be used as the order parameter to distinguish the volume law phase from the other two area law phases. Assuming the dynamical exponent $z=1$, for S_a we have[6]:

$$S_a(p, L, t) = G((p - p_c)L^{1/\nu}, t/L), \tag{10}$$

where $G(x)$ is some unknown function. $\tilde{S}_a$ has a similar scaling form.

We now present our numerical results. We study system sizes up to 512 qubits and average over 10^5 random quantum trajectories. We start with the $|0\rangle^{\otimes N}$ state and let the circuit run for $2N$ time steps for the system to reach the steady state. We have explicitly verified that saturation is reached before $t=2N$. After entangling the ancilla

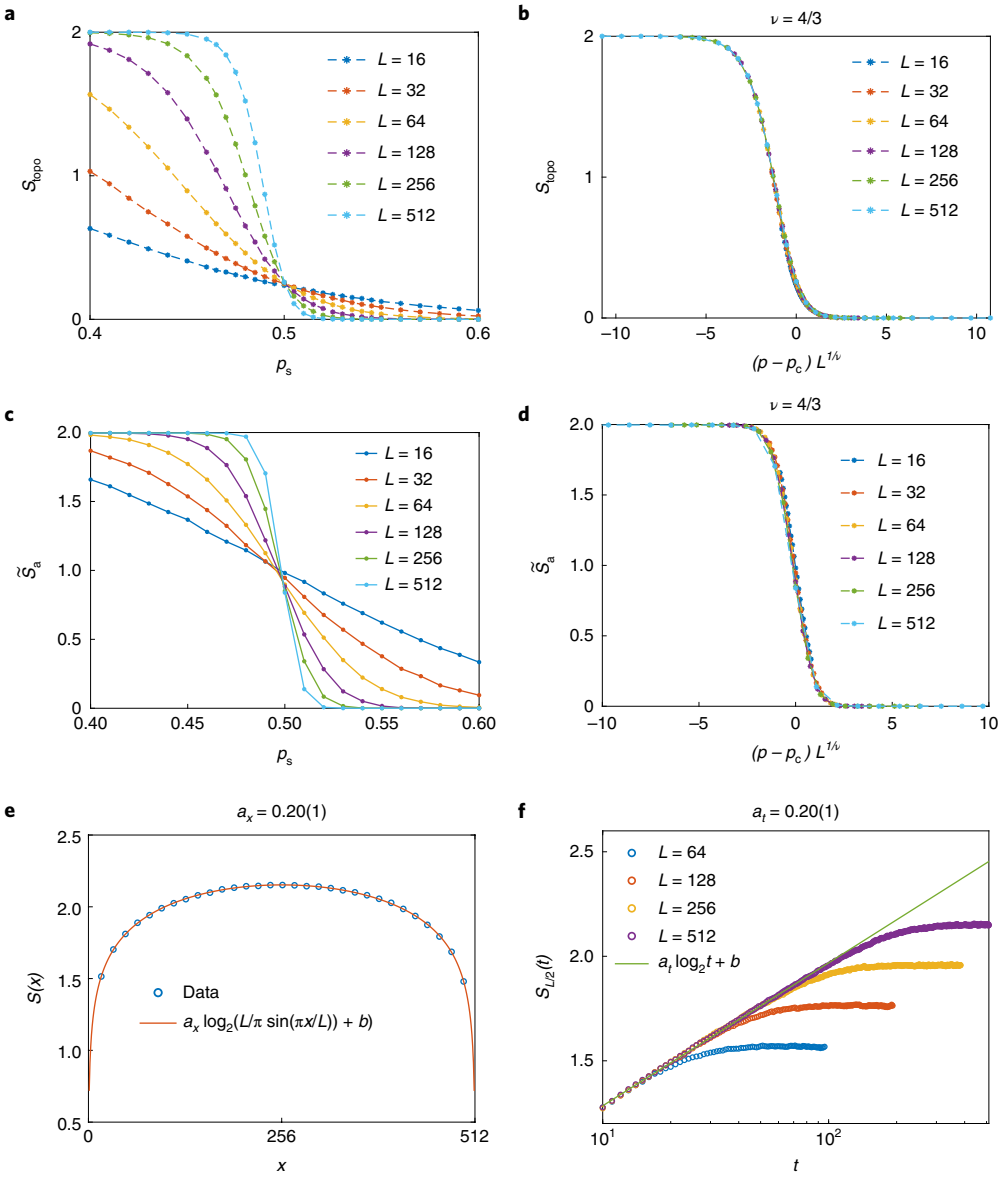

Fig. 3 | The numerical results pertaining to the tricritical point at $p_u = 0$. a, S_{topo} near the tricritical point versus p_s. **b**, Scaling collapse of the data in **a**. **c**, $\tilde{S}_a$ measured $t = N$ time steps after scrambling. **d**, Scaling collapse of the data in **c**. **e**, The entanglement entropy of the $[0, x]$ segment of the chain $S(x, L)$ at late times for $p = p_c$ and $L = 512$. **f**, The entanglement entropy of the half chain versus time for $p_s = p_c$. All entropies are in units of $\log_2$. See Supplementary Section 8 for an analytical derivation of the a coefficient using the percolation map.

qubit, we simulate the system for an additional $O(N)$ time steps to calculate S_a (as explained above).

Figure 3 shows numerical results along the $p_u = 0$ line. Figure 3a,c shows the steady-state value of S_{topo} and $\tilde{S}_a$ versus p_s for different system sizes. As is evident from both diagrams, there is a clear continuous phase transition at $p_c = 1/2$ in the thermodynamic limit. A simple argument based on duality shows that if there is a continuous phase transition between the trivial and topological phase, it has to be at $p_s = 1/2$. This duality argument is provided in Supplementary Section 6. We find that S_a seems to be unable to capture the area law to area law phase transition at $p_u = 0$, at least for numerically accessible systems sizes. On the other hand, from collapsing the data near the critical point $p_c = 1/2$, we find that $\nu = 4/3$ results in a near perfect collapse (Fig. 3c,d).

Figure 3e shows the steady-state value of entanglement entropy $S(x)$ of the subregion $[1, x]$ at the critical point $p_u = 0$ and $p_s = 1/2$, for $L = 512$. As shown, the entanglement entropy fits the CFT form of equation (7) with $a_x = 0.20(1)$. The number in the parentheses is the uncertainty in the last digit. See Methods for more details on how the errors are estimated.

Figure 3f shows the entanglement entropy of the half chain versus time at $p = p_c$ for different chain sizes. The entanglement entropy grows logarithmically with time, until the finite size effects show up. By comparing the corresponding fitted analytical expressions we find $a_t = a_x = 0.20(1)$.

We note that the values of ν, z, a_x and a_t at the $p_u = 0$, $p_s = 1/2$ transition agree with the values of our other random measurement-based quantum circuit model presented in Supplementary Section 9, which in turn maps to (two copies of) the standard classical link percolation problem on the square lattice. Our results are thus consistent with the $p_u = 0$, $p_s = 1/2$ transition studied in Fig. 3 being governed by (two copies of) the standard classical percolation fixed point.

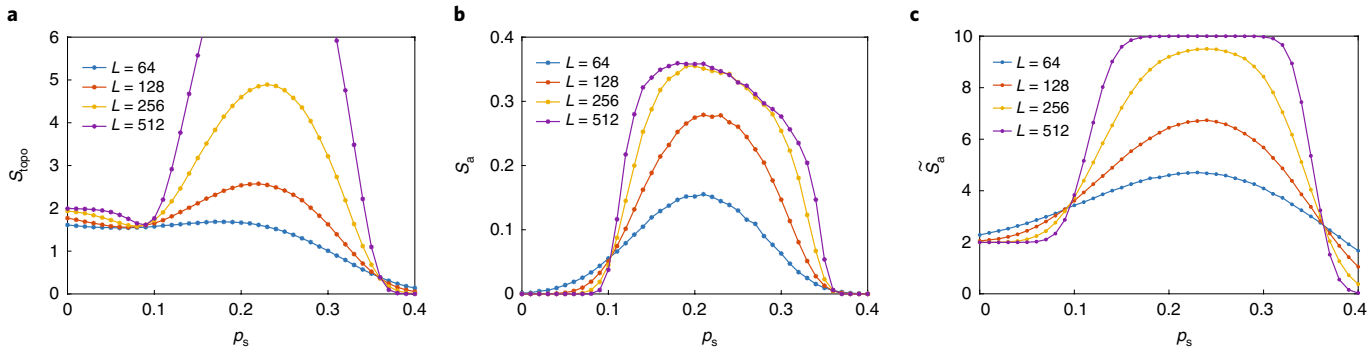

Fig. 4 | The phase transitions across the $p_u = 0.3$ line. a, S_{topo} verses p_s. **b**, S_a measured $t = N$ time steps after it was entangled versus p_s. **c**, S_a measured $t = N$ time steps after it was entangled versus p_s. In all panels, the first crossing corresponds to the phase transition from the SPT phase into the volume law phase, whereas the second crossing corresponds to the phase transition from the volume law phase to the trivial phase. The critical points are also marked on the phase diagram in Fig. 1b.

We now proceed to the case with unitary dynamics $p_u \neq 0$. Figure 4 shows S_{topo}, S_a and $\tilde{S}_a$ versus p_s for the fixed value of $p_u = 0.3$. For $p_s = 0$, the system is in the topological phase, as can be seen from Fig. 4a. By increasing p_s, the entropies exhibit a continuous phase transition to the volume law phase at first, and then another continuous phase transition to the trivial phase.

By using analogous plots for different values of p_u, we can determine the 2D phase diagram in the (p_s, p_u) space. The result is illustrated in Fig. 1b. Note that as the probability of measuring a stabilizer is $1 - p_u - p_s$, the phase diagram is restricted to the region $p_u + p_s \leq 1$. The data points in the plot have been extracted using numerical simulations and the schematic phase diagram is then drawn based on them. For more detailed results used to obtain the phase diagram see Supplementary Section 11.

The SPT/volume law phase boundary intersects the p_u axis at $p_u = 0.355(3)$ and the volume law/trivial phase boundary ends at $p_u = 0.663(4)$ on the $p_u + p_s = 1$ line. Our numerical simulations demonstrate that the volume law phase still exists for p_u as low as 0.1. Unfortunately, clearly detecting the transition from the SPT to volume law phases requires increasingly large system sizes as p_u is lowered (see Supplementary Section 10 for details). Therefore, we extrapolate the phase diagram for smaller values of p_u. By following the trend of the data points, it seems that the volume law phase survives all the way down to $p_u = 0$, hence suggesting that the critical point at $p_s = 0.5$ and $p_u = 0$ is actually a tricritical point. This in turn means that at $p_s = 1/2$, arbitrarily sparse random Clifford gates in the quantum circuit can still drive the system into the volume law phase.

By using the scaling form in equation (9) and collapsing the data, we can extract the correlation length critical exponent ν along the phase boundaries. Taking into account the margins of error, our numerical results are consistent with $\nu = 4/3$ everywhere along the phase boundaries (see Supplementary Section 11 for the corresponding plots and numerical values). However $a_x = a_t$ changes considerably along the phase boundaries at the largest system sizes we have studied. If the $a_x = a_t$ that we extract are close to their values in the thermodynamic limit, this suggests that the volume law to area law critical lines may be related to two copies of the classical percolation fixed point by marginal deformations.

Entanglement phase transitions involving topological or SPT phases also seem to be closely related to quantum error correction. In particular, the rapid stabilizer measurements are reminiscent of syndrome measurements in active error correction schemes. Moreover, random single-qubit measurements can be viewed as faulty syndrome measurements or qubit decoherence, whereas unitary dynamics models the random noise affecting the qubits. In this context, 'entanglement phase transitions' could be related to 'error thresholds' beyond which the long-range entanglement structure of the code space, which is responsible for the topological protection of the encoded information, is entirely lost, rendering recovery of logical information impossible. Within this framework, our results might have natural applications to quantum error correcting codes. Note that this is a different analogy to quantum error correction than the one presented in refs. [5,8], where the volume law phase is considered to be a quantum error correcting code.

Online content

Any methods, additional references, Nature Research reporting summaries, source data, extended data, supplementary information, acknowledgements, peer review information; details of author contributions and competing interests; and statements of data and code availability are available at https://doi.org/10.1038/s41567-020-01112-z.

Received: 24 April 2020; Accepted: 29 October 2020;
Published online: 4 January 2021

References

1. Skinner, B., Ruhman, J. & Nahum, A. Measurement-induced phase transitions in the dynamics of entanglement. *Phys. Rev. X* **9**, 031009 (2019).
2. Li, Y., Chen, X. & Fisher, M. P. A. Quantum Zeno effect and the many-body entanglement transition. *Phys. Rev. B* **98**, 205136 (2018).
3. Chan, A., Nandkishore, R. M., Pretko, M. & Smith, G. Unitary-projective entanglement dynamics. *Phys. Rev. B* **99**, 224307 (2019).
4. Li, Y., Chen, X. & Fisher, M. P. A. Measurement-driven entanglement transition in hybrid quantum circuits. *Phys. Rev. B* **100**, 134306 (2019).
5. Gullans, M. J. & Huse, D. A. Dynamical purification phase transition induced by quantum measurements. *Phys. Rev. X* **10**, 041020 (2020).
6. Gullans, M. J. & Huse, D. A. Scalable probes of measurement-induced criticality. *Phys. Rev. Lett.* **125**, 070606 (2020).
7. Vasseur, R., Potter, A. C., You, Y.-Z. & Ludwig, A. W. W. Entanglement transitions from holographic random tensor networks. *Phys. Rev. B* **100**, 134203 (2019).
8. Choi, S., Bao, Y., Qi, X.-L. & Altman, E. Quantum error correction in scrambling dynamics and measurement-induced phase transition. *Phys. Rev. Lett.* **125**, 030505 (2020).
9. Szyniszewski, M., Romito, A. & Schomerus, H. Entanglement transition from variable-strength weak measurements. *Phys. Rev. B* **100**, 064204 (2019).
10. Tang, Q. & Zhu, W. Measurement-induced phase transition: a case study in the nonintegrable model by density-matrix renormalization group calculations. *Phys. Rev. Res.* **2**, 013022 (2020).
11. Jian, C.-M., You, Y.-Z., Vasseur, R. & Ludwig, A. W. W. Measurement-induced criticality in random quantum circuits. *Phys. Rev. B* **101**, 104302 (2020).
12. Cao, X., Tilloy, A. & De Luca, A. Entanglement in a fermion chain under continuous monitoring. *SciPost Phys.* **7**, 24 (2019).
13. Lopez-Piqueres, J., Ware, B. & Vasseur, R. Mean-field entanglement transitions in random tree tensor networks. *Phys. Rev. B* **102**, 064202 (2020).

14. Bao, Y., Choi, S. & Altman, E. Theory of the phase transition in random unitary circuits with measurements. *Phys. Rev. B* **101**, 104301 (2020).
15. Piroli, L., Sünderhauf, C. & Qi, X.-L. A random unitary circuit model for black hole evaporation. *J. High Energy Phys.* **2020**, 63 (2020).
16. Zabalo, A. et al. Critical properties of the measurement-induced transition in random quantum circuits. *Phys. Rev. B* **101**, 060301 (2020).
17. Rossini, D. & Vicari, E. Measurement-induced dynamics of many-body systems at quantum criticality. *Phys. Rev. B* **102**, 035119 (2020).
18. Fan, R., Vijay, S., Vishwanath, A. & You, Y.-Z. Self-organized error correction in random unitary circuits with measurement. Preprint at https://arxiv.org/abs/2002.12385 (2020).
19. Nahum, A. & Skinner, B. Entanglement and dynamics of diffusion-annihilation processes with Majorana defects. *Phys. Rev. Res.* **2**, 023288 (2020).
20. Hastings, M. B. Topological order at nonzero temperature. *Phys. Rev. Lett.* **107**, 210501 (2011).
21. Chen, X., Gu, Z.-C., Liu, Z.-X. & Wen, X.-G. Symmetry protected topological orders and the group cohomology of their symmetry group. *Phys. Rev. B* **87**, 155114 (2013).
22. Raussendorf, R. & Briegel, H. J. A one-way quantum computer. *Phys. Rev. Lett.* **86**, 5188 (2001).
23. Zeng, B., Chen, X., Zhou, D.-L. & Wen, X.-G. *Quantum Information Meets Quantum Matter* (Springer, 2019); https://doi.org/10.1007/978-1-4939-9084-9
24. Son, W. et al. Quantum phase transition between cluster and antiferromagnetic states. *Europhys. Lett.* **95**, 50001 (2011).
25. Santos, L. H. Rokhsar-Kivelson models of bosonic symmetry-protected topological states. *Phys. Rev. B* **91**, 155150 (2015).
26. Tsui, L., Huang, Y.-T., Jiang, H.-C. & Lee, D.-H. The phase transitions between $Z_n \times Z_n$ bosonic topological phases in 1 + 1D, and a constraint on the central charge for the critical points between bosonic symmetry protected topological phases. *Nucl. Phys. B* **919**, 470–503 (2017).
27. Zeng, B. & Wen, X.-G. Gapped quantum liquids and topological order, stochastic local transformations and emergence of unitarity. *Phys. Rev. B* **91**, 125121 (2015).
28. Zeng, B. & Zhou, D.-L. Topological and error-correcting properties for symmetry-protected topological order. *Europhys. Lett.* **113**, 56001 (2016).
29. Fromholz, P., Magnifico, G., Vitale, V., Mendes-Santos, T. & Dalmonte, M. Entanglement topological invariants for one-dimensional topological superconductors. *Phys. Rev. B* **101**, 085136 (2020).
30. Calabrese, P. & Cardy, J. Entanglement entropy and conformal field theory. *J. Phys. A* **42**, 504005 (2009).
31. Li, Y., Chen, X., Ludwig, A. W. W. & Fisher, M. P. A. Conformal invariance and quantum non-locality in hybrid quantum circuits. Preprint at https://arxiv.org/abs/2003.12721 (2020).

Methods

Binary representation of the stabillizer circuit. We use the binary representation of the stabilizer formalism to simulate the Clifford circuits studied in this work. This representation is based on the observation that, up to some phase factor, any Pauli string operator s over N qubits can be uniquely mapped to a binary vector $\mathbf{w} = (\mathbf{u}, \mathbf{v}) \in \mathbb{Z}_2^{2N}$ where $\mathbf{u}, \mathbf{v} \in \mathbb{Z}_2^N$ and

$$s = e^{i\theta} \prod_{i=1}^{N} X_i^{u_i} \prod_{i=1}^{N} Z_i^{v_i} \tag{11}$$

If Pauli string operators s_1 and s_2 correspond to vectors $\mathbf{w}_1$ and $\mathbf{w}_2$, their multiplication $s_1 s_2$ corresponds to $\mathbf{w}_1 + \mathbf{w}_2$. Moreover, $[s_1, s_2] = 0$ if, and only if, $\mathbf{w}_1^T g \mathbf{w}_2 = 0$, where $\mathbf{w}^T$ stands for $\mathbf{w}$ transposed and g is the $2N \times 2N$ matrix defined as

$$g = \left(\begin{array}{c|c} 0_{N\times N} & \mathbb{1}_{N\times N} \\ \hline \mathbb{1}_{N\times N} & 0_{N\times N} \end{array} \right).$$

It is also easy to apply Clifford unitaries in the binary representation. Let U be a unitary in the Clifford group. Since U belongs to the Clifford group, the images of X_i and Z_i under U (that is, $UX_iU^\dagger$ and $UZ_iU^\dagger$) are themselves Pauli string operators and have binary representations in $\mathbb{Z}_2^{2N}$. Let M_U be the $2N \times 2N$ matrix whose first and second N columns correspond to the images of X_i and Z_i under U respectively, for $i = 1, \cdots, N$. It is easy to see that, if $\mathbf{w}$ is the binary representation of a Pauli string s, the binary representation of $UsU^\dagger$ would be given by the matrix multiplication $M_U \mathbf{w}$ in $\mathbb{Z}_2$.

Given a stabilizer set R, an $N \times 2N$ stabilizer matrix M_R can be formed by taking the binary representation of the elements of R as its rows. For example, the stabilizer matrix that corresponds to the state $|0\rangle^{\otimes N}$ is given as

$$M_R = (0_{N\times N} | \mathbb{1}_{N\times N}) \tag{13}$$

One may keep track of the phase factors using an additional N element vector, but as we are interested in the entanglement structure, which is independent of the phase factors (see Lemma 1 in Supplementary Information), we ignore the phase factor in what follows.

In our numerics, we use the stabilizer matrix of the system to keep track of the entanglement dynamics of the system. As was discussed above, applying a unitary U would transform M_R to $M_R M_U^T$ where M_U is the binary representation of U and T stands for transpose (note that the stabilizers are stored as the rows of M_R rather than its columns). It is also straightforward to keep track of the Clifford measurements owing to the Gottesman–Knill theorem[32,33]. Let s_* represent the Pauli string operator that is being measured. First we find the stabilizers in R that do not commute with s_*, which can be done efficiently by computing $M_R g s_*$ with g as defined in equation (12). If s_* commutes with every stabilizer in R, then measuring it has no effect on the state of the system. On the other hand, if s_* does not commute with some stabilizers in R, say $s_1, \cdots, s_m$, the stabilizer set of the system after measuring s_* can be obtained by replacing s_1 with $\pm s_*$ and s_i with $s_1 s_i$ for $i = 2, \cdots, m$, where the $\pm$ sign is chosen at random. As we are ignoring the phase factors in the binary representation, this amounts to replacing the row corresponding to s_1 with the binary representation of s_* and adding the binary representation of s_1 to the rows corresponding to $s_2 \cdots s_m$.

To sample the three-qubit symmetric Clifford unitary set, we use the procedure outlined in ref. [4] to generate all possible binary representations of three-qubit Clifford unitaries and then choose the symmetric subset by explicitly checking whether a unitary respects the $\mathbb{Z}_2 \times \mathbb{Z}_2$ symmetry.

As the last remark in this section, we note that given the stabilizer matrix M_R, the entanglement entropy of a subset A of the qubits can obtained via[34]:

$$S_A = \text{rank}\,(M_R|_A) - n_A, \tag{14}$$

where $M_R|_A$ is the submatrix of M_R obtained via keeping only the columns that correspond to the qubits in A, n_A is the number of qubits in A and the rank is computed in $\mathbb{Z}_2$.

Estimating the errors. In this section, we briefly summarize the procedure that was used to estimate the numerical values of parameters and their corresponding errors.

The critical value p_c can be found by plotting the order parameter for different system sizes and locating the scale-invariant point at which all the curves for different system sizes cross. The reported value of p_c corresponds to the crossing point of the order parameter curves for $L = 512$ and $L = 256$, whereas the curves for smaller system sizes are used to estimate the error. We find $p_c(L)$ for $L = 512$, 256 and 128, where $p_c(L)$ is defined as the crossing point between curves of system sizes L and $L/2$. The y-axis intercept of the linear fit to $p_c(L)$ as a function of $1/L$ gives an estimate for $p_c(L \to \infty)$. The error in p_c is then estimated by the difference between the extrapolated value $p_c(L \to \infty)$ and its value at $L = 128$. We use S_a as the order parameter to detect the phase transition from SPT to volume law entangled phase, while we use S_{topo} for the phase transition from the volume law entangled phase to the trivial phase. The reason for using two different order parameters is that although S_{topo} has less noise than the ancilla order parameter, one has to go to larger system sizes to properly detect the SPT–volume law phase transition using this order parameter. On the other hand, although S_a has to be averaged over a higher number of realizations, it displays a sharper crossing compared with S_{topo} or $\tilde{S}_a$ (Supplementary Section 11).

The value of correlation length critical exponent ν is found from the data collapse. Assume that a certain quantity, say S_a, has the following finite size scaling form:

$$S_a(p, L) = F((p - p_c)L^{1/\nu}) \tag{15}$$

for some arbitrary function F. It follows that if one plots S_a as a function of $(p - p_c)L^{1/\nu}$, for the right choice of ν, all the data points would collapse on the $y = F(x)$ curve. To find the best collapse, we use the objective function $\epsilon(\nu)$ defined as:

$$\epsilon(\nu) = \frac{1}{n-2} \sum_{i=2}^{n-1} \left(y_i - \bar{y}_i\right)^2, \tag{16}$$

where

$$\bar{y}_i = \frac{(x_{i+1} - x_i)y_{i-1} - (x_{i-1} - x_i)y_{i+1}}{x_{i+1} - x_{i-1}}, \tag{17}$$

with $x_i = (p_i - p_c)L_i^{1/\nu}$ and $y_i = S_a(p_i, L_i)$. Here i labels the ith data point (including system sizes $L = 64$, 128, 256 and 512) sorted on the basis of their x value such that $x_1 < x_2 < \cdots < x_n$, and n denotes the total number of data points. $\bar{y}_i$ is the expected value of y_i if it was on the line passing through the two adjacent data points. For the perfect collapse and in the limit of infinitely close data points, $\epsilon(\nu)$ would vanish. To obtain the best collapse, we find the value ν^* that minimizes the objective function $\epsilon(\nu)$ for a given set of numerical data. To estimate the error, we find the ν interval for which $\epsilon(\nu) < 2\epsilon(\nu^*)$.

The numerical values of a_t and a_x (equations (7) and (8)) are obtained by fitting the numerical data for $L = 512$ to the analytical expressions via the method of least squares. As these equations are field theory results and are valid only in length scales much larger than lattice spacing, we exclude data points corresponding to first and last ten sites before fitting the data to equation (7). As for equation (8), we exclude data points for $t < 10$ as well as data points close to the saturation value of the half-chain entropy, $S_{L/2}(t) > 0.9 S_{L/2}(\infty)$. Let ε_1 denote the error that characterizes the fit quality. There is also a systematic source of error related to finite size effects, which we denote ε_2. To estimate ε_2, we evaluate $a_x(L)$ and $a_t(L)$ for $L = 128$, 256 and 512, find the y-axis intercept of the linear fit to $a_x(L)$ (and $a_t(L)$) as a function of $1/L$ and then estimate ε_2 as the difference between the y-axis intercept and the parameters evaluated at $L = 128$. The reported error is then $\max(\varepsilon_1, \varepsilon_2)$.

Data availability

The data plotted in the figures of this Article that support the findings of this study are available via Zenodo at https://doi.org/10.5281/zenodo.4031884.

Code availability

The source codes used to run the simulations of the symmetric random quantum circuit studied in this Article are available via Zenodo at https://doi.org/10.5281/zenodo.4031884.

References

32. Gottesman, D. The Heisenberg representation of quantum computers. In *Proc. 22nd International Colloquium on Group Theoretical Methods in Physics* (eds Corney, S. P. et al.) 32–43 (International, 1998); https://arxiv.org/abs/quant-ph/9807006
33. Nielsen, M. A. & Chuang, I. *Quantum Computation and Quantum Information* (Cambridge Univ. Press, 2002).
34. Nahum, A., Ruhman, J., Vijay, S. & Haah, J. Quantum entanglement growth under random unitary dynamics. *Phys. Rev. X* **7**, 031016 (2017).

Acknowledgements

We thank M. Hafezi, H. Dehghani and A. Nahum for helpful comments, and M. Gullans and D. Huse for suggesting the modified ancilla order parameter and for discussions regarding its saturation value in the topological phase. We acknowledge the University of Maryland supercomputing resources (http://hpcc.umd.edu) made available for conducting the research reported in this paper. A.L. and M.B. are supported by NSF CAREER (grant number DMR- 1753240), the Alfred P. Sloan Research Fellowship and JQI-PFC-UMD. Y.A. is supported by National Science Foundation grant number NSF DMR1555135 and JQI-NSF-PFC.

Author contributions

All authors contributed equally to this work.

Competing interests
The authors declare no competing interests.

Additional information
Supplementary information is available for this paper at https://doi.org/10.1038/s41567-020-01112-z.

Correspondence and requests for materials should be addressed to A.L.

Peer review information *Nature Physics* thanks Xiao Chen, Masaki Oshikawa and Brayden Ware for their contribution to the peer review of this work.

Reprints and permissions information is available at www.nature.com/reprints.